Chapter IV

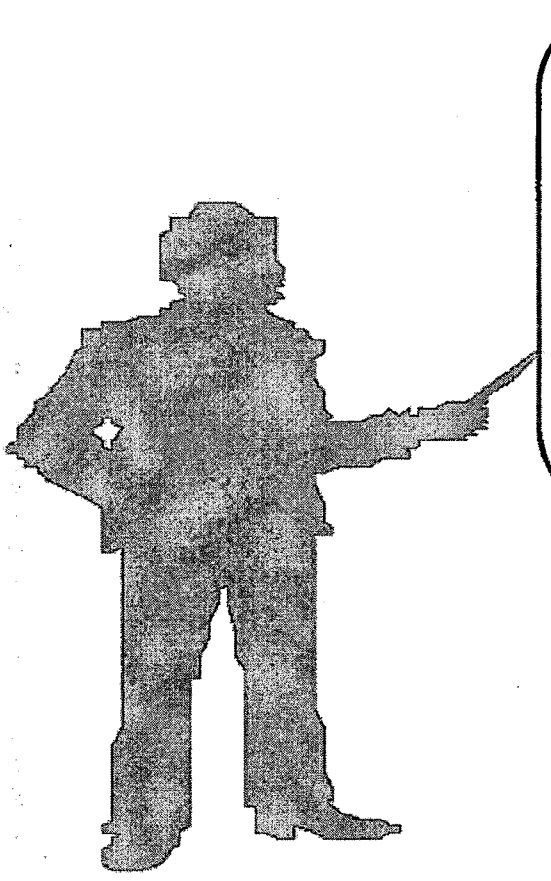

Development and Characterization of Doxorubicin Loaded Polymersomes (PolyDOX) and Preliminary Cell line Studies on C6 Glioma Cells

4.1. Introduction

Nanotechnology is an exciting approach in the development of new therapeutics, expected to change the landscape of pharmaceutical companies (Farokhzad and Langer 2009; Whitesides 2003). In this context, block copolymer vesicles are considered as promising drug delivery systems, mainly due to high membrane stability that overcomes most of the challenges encountered with similarly structured liposomes (Discher et al., 1999; Ghoroghchian et al., 2005; Ahmed et al., 2006; Discher et al., 2007; Adams et al., 2008). The chemical versatility of block copolymers offers the additional advantage of almost infinite possibilities for the introduction of a specific biofunctionality with properties targeting a defined disease (Nasongkla et al., 2006; Peer and Margalit 2004; Opsteen et al., 2007; Hammer et al., 2008; Sun et al., 2009; You and Schlaad 2006). In addition to a high drug loading capacity and an adequate stability in bloodstream circulation, the capacity of a colloidal drug delivery system to selectively accumulate the drug at the site of action is of major importance to improve therapeutic efficiency and reduce side effects (Langer 1998; Peer et al., 2007). A large range of targeting ligands such as antibodies, peptides, nucleic acids or carbohydrates has now been identified to selectively bind biological targets. However, integration of these binding agents onto nano-carriers often requires tedious chemical reactions and decreases the nanoparticle stability and, as a consequence, blood half-life. The originality of our strategy consists of using a polymer moiety that acts as a bio-receptor and a stabilizing agent in the nanoparticle construction. Hyaluronan (HYA or HA), a linear glycosaminoglycan consisting of alternating D-glucuronic acid and N-acetyl D-glucosamine units has been selected for both its physicochemical and biological properties. Hyaluronan is a highly water-soluble polymer due to its polyelectrolyte behavior and acts thus as an efficient electrosteric stabilizer when grafted at the surface of nanoparticles. More importantly, hyaluronan is known as a major ligand for CD44, a type 1 transmembrane glycoprotein upregulated in certain cancers (Girish and Kemparaju 2007). Targeting to CD44 with hyaluronan or anti-CD44 antibodies grafted onto nanocarrier systems such as liposomes has been performed by several authors for cancer therapies (Hu et al., 1999; Peer and Margalit 2004; Eliaz and Szoka 2001). However, drawbacks related to liposome surface

chemistry include a restricted chemical accessibility and a multipoint attachment of the HYA to the surface when coupling was performed covalently *via* glucuronic carboxylates.

Additionally, lipid-based vesicles generally present the major disadvantage of a poor stability in physiological conditions, even if recent examples of vesicles based on pegylated lipids are show improved properties (Lewanski and Stewart 1999, Immordino et al., 2006). However, surface functionalization with targeting moieties such as hyaluronan even further compromises their colloidal stability and their use in vivo. Polymer vesicles can overcome this main challenge and have been demonstrated to be act as robust containers (Bermudez et al., 2002; Discher and Eisenberg 2002) able to encapsulate both hydrophilic and hydrophobic molecules (Ahmed et al., 2006). Indeed, their membrane physical properties are directly correlated to their thickness, which can be controlled by the block copolymer molecular weight. Among the different block copolymer vesicles studied so far, polypeptide-based vesicles present several advantages. Their building blocks, which are biocompatible by nature, are mimicking the behavior of proteins and allow driving the self-assembly process with an accurate control of their secondary structure. For example, it has been shown that vesicles can be highly stabilized due to the rod-like conformation of polypeptide chains forming the hydrophobic part of the membrane (Bellomo et al., 2004; Rodríguez-Hernández et al., 2005). In a recent and relevant work, Deming and coworkers reported the formation of poly(L-lysine)-*block*-poly(arginine) block copolymers (Holowka et al., 2007). Interestingly, the poly(arginine) segment was used both to direct structure for vesicle formation and to provide biofunctionality to efficient intracellular delivery of the vesicles, mimicking the arginine rich sequence identified to be relevant in protein-transduction domains (Calnan et al., 1991).

4.2. Materials

Doxorubicin HCl was purchased from RPG Life Sciences Limited, Mumbai (India). Dulbecco's modified Eagle's medium (DMEM) (Sigma-Aldrich, France), fetal calf serum (FCS), antibiotics (penicillin, streptomycin and amphotericin B) (Gibco, Invitrogen corporation, France) and MTT (3-(4,5-dimethyathiazol-2-yl)-2,5-diphenyl

tetrazolium bromide) were purchased from Sigma-Aldrich, France. C6 Cells were taken from in-house stock in Laboratoire de Résonance Magnétique des Systèmes Biologiques UMR 5536 CNRS, Bordeaux, FRANCE.

4.3. Formulation DOX loaded polymersomes (PolyDOX)

DOX loading was performed at different feed weight ratio of DOX: $PBLG_{23}$-*b*-HYA_{10} by nanoprecipitation method. DOX and block copolymer was dissolved in warm DMSO, then tris buffer (10 mM, 154mM ionic strength with pH = 7.4) was injected at 18 mL/h (with a 5 ml syringe) or 36 mL/h (with a 10 ml syringe) in DMSO (block copolymer concentration = 0.5 wt %) with continuously stirring at 55°C for final concentration of copolymer 1mg/mL (0.1 wt %). The unloaded DOX and DMSO were removed by dialysis (MWCO = 2000 g/mol, 6 Spectra/Por® membrane) against tris buffer (10 mM, 154mM ionic strength with pH = 7.4). Samples were dialyzed against 1000 times of outside medium, with 3 changes of this medium in 4h. Loading content of DOX was determined after breaking of PolyDOX in a DMSO: tris buffer (80:20) mixture. After centrifugation at 37°C for 30 minutes, the sample was vortexed (10 minutes). Then, sample was filtered (0.45µm, Nylon) and subjected for UV measurement at λ_{max} = 485 nm. Quantification was performed from the calibration curve of DOX in DMSO: tris buffer (80:20).

$$Loading\ Content = \frac{Drug\ amount\ in\ loaded\ vesicle}{Amount\ of\ vesicle} \times 100$$

$$Loading\ Efficiency = \frac{Drug\ Amount\ in\ Loaded\ Vesicle}{Intial\ Amount\ of Drug} \times 100$$

4.4. Characterization

4.4.1. Dynamic light scattering

Dynamic light scattering (DLS) experiments were performed using ALV Laser Goniometer, which consists of 22mW HeNe linear polarized laser with 632.8 nm wavelength and an ALV-5000/EPP Multiple Tau Digital Correlator with 125 ns initial sampling time. The samples were kept at constant temperature (25°C) during all the

experiments. The accessible scattering angle range is from 10° up to 150°. The solutions were introduced into 10 mm diameter glass cells. The minimum sample volume required for the experiment was 1 ml. The data acquisition was done with the ALV-Correlator Control Software, and the counting time varied for each sample was 300s. Water was thoroughly filtered with 0.1μm filters and directly employed for the preparation of the solutions.

4.4.2. Microscopy

Freeze-Fracture Transmission Electron Microscopy (FF-TEM) experiments, a drop of the water solution of $PBLG_{23}$-*b*-HYA_{10} (0.1mg/mL) was placed between two copper planchettes of a sandwich holder and freezed by plunging into liquid propane. Sample was then fractured at -150°C and pressure of the order of 10^{-6} mbar in a BAF 300 Balzers apparatus. The fractured surfaces were replicated with platinum evaporated at a 45°angle, followed by carbon deposition normal to the fracture surface to increase mechanical strength. The copper planchettes were dissolved in chromerge® (a mixture of chromic acid, sulphuric acid and water). The detached replicas were then rinsed with water and cleaned from copolymer with DMSO, before being collected on the 200 mesh copper grid. Observations were made with a FEI Tecnai 12 Microscope working at 120keV.

Atomic force microscopy (AFM) was performed under air at 25°C using a Nanoscope IIIa microscope in tapping-mode. Commercially available silicon tip probes had a spring constant of 42N m^{-1}, a resonance frequency of 285 kHz, and a typical radius of curvature in the 8^{-10} nm range. Both topography and phase signal images were recorded with 512 × 512 data points. All samples were prepared on mica by spin-coating at 700 rpm for 10 minutes and allowed to dry for two days at room temperature.

4.4.3. pH effect on zeta potential and particle size of PolyDOX

The effect of pH on the colloidal behavior of polymersomes was investigated by determining both the zeta potential and the hydrodynamic radius (Malvern Zetasizer HS 3000) for pHs between 3 and 8. The pH was adjusted with 0.1M HCL and 0.1M NaOH solution.

4.4.4. *In vitro release studies*

In vitro DOX release was investigated at pH 7.4 (10mM tris buffer) and pH 5.5 (100mM acetate buffer). A defined amount of PolyDOX was introduced in a dialysis tube [Spectra/Por® Float-A-LyzerTM, MWCO 25000 g/mol, diameter: 10mm, Volume: 10 mL). Dialysis tube was placed into *in vitro* release medium, 50 mL tris buffer (pH 7.4) or 50 mL acetate buffer (pH 5.5). Whole assembly was kept at 37±2°C and covered by parafilm to avoid evaporation. The sink conditions were maintained by replacing release media with fresh media at each sampling point. The amount of drug released was estimated from the residual drug in the vesicles by absorption measurement at λ = 485 nm. The drug concentration was linearly related to the measured absorbance. The amount of the drug released was calculated from the amount of drug initially present in the vesicles and the amount of drug retained in the vesicles at each sampling point.

4.5. Stability studies

PolyDOX prepared at different feed weight ratios (DOX/copolymer) were investigated for stability at room temperature (RT) and at 4°C temperature for days. PolyDOX formulations were divided into two batches, one being kept at RT and the other one at 4°C. Loading content and hydrodynamic radius were determined as per above mentioned procedure. Before analysis, 4°C samples have been vortexed for one minute.

4.6. Lyophilization process

PolyDOX formulations were investigated for lyophilization process. PolyDOX suspensions were frozen with liquid nitrogen in 10 mL vials and then lyophilized (CHRIST, ALPHA 1-2 LD plus, BIOBLOCK SCIENTIFIC). After 48h, samples were removed from the lyophilizer, reconstituted with the required amount of tris buffer and vortexed for 10min. Loading content and hydrodynamic radius were determined as per above mentioned procedure, before and after the lyophilization.

4.7. Cell line studies on C6 rat glioma cells

4.7.1. Cell culture

Cell culture experiments were performed on rat C6 glioma cell line, grown in Dulbecco's modified Eagle's medium (DMEM) containing 5% fetal calf serum (FCS). C6 glioma cells (5×10^5) were placed onto 10 cm diameter Falcon dishes and grown in 10mL of DMEM cell medium with 5% FCS, penicillin (100 U/mL), streptomycin (100μg/mL) and amphotericin B (25μg/mL) (Invitrogen Corporation) in a water saturated incubator at 37°C in an atmosphere of 5% CO_2/95% air. DOX concentration in polymersomes was adjusted to be the same as free DOX in whole cell line experiments.

4.7.2. Effect on cell morphology after treatment

The 5μM equivalent DOX concentrations of free DOX and PolyDOX were added to the cell culture and incubated at 37°C in an atmosphere of 5% CO_2/95% air for 24 h. Following drug treatment, the plates were observed under a Zeiss fluorescence microscopy (Germany) to detect morphological changes.

4.7.3. Cell viability

C6 cells were seeded at a density of 15×10^4 cells/well in 24-wells transparent plates and incubated for 24 h. The cell viability was determined by the MTT (3-(4,5-dimethyathiazol-2-yl)-2,5-diphenyl tetrazolium bromide) assay. This assay is based on the measurement of the dehydrogenase activity of viable cells by the reduction of the tetrazolium salt MTT to a blue product formazan. A stock solution of 5 mg/ml MTT was prepared in PBS and at the designated time intervals, ten percent MTT was added and incubated for 45 min at 37°C. The medium was removed and the wells were washed once with 1 mL PBS and cell pellets were collected in tube by centrifugation (180g for 10 min). Supernatant PBS was removed and 1 mL of DMSO was added for solubilization of formazan by centrifugation (180g for 10 min). Each sample was finally analyzed by spectrophotometry (U-2800A, HITACHI) with absorbance detection at 570 nm. Control samples were performed with untreated cells viability. In parallel, control cells were

collected by sterile cells scraper and counted on a Malassez slide after trypan blue staining.

4.7.4. Cell uptake studies (Fluorescence Microscopy)

C6 cells were cultured at a density of 15 × 10^4 cells/well in 4-well plastic dishes (16mm) containing 12mm coverslips for 24h. Free DOX (5μM) and loaded DOX (5μM) were incubated for 6 and 24h at 37°C in an atmosphere of 5% CO_2/95% air. After the designated time intervals, the cells were washed 2 times with PBS. The cells on coverslips were fixed 30 min with 4% paraformaldehyde (PFA) in PBS at room temperature. Coverslips were then mounted on slides with mowiol and viewed by Zeiss fluorescence microscopy (Germany).

4.7.5. Cell uptake studies (Flow Cytometry)

C6 cells were cultured at a density of 15 × 10^4 cells/well in petri dishes (35mm) for 24h. Free DOX (5μM) and loaded DOX (5μM) were incubated for 6, 24 and 48h at 37°C in an atmosphere of 5% CO_2/95% air. After designated time intervals, cell medium was removed and the cells were washed one time with 1 mL PBS. Cells were then scraped off by sterile cell scraper and collected by spun down (180g for 10 min). The pellet was homogeneously resuspended in 1 mL of RPMI and cellular sample was analyzed with a fluorescent assay cell sorter (FACS Calibur; Becton-Dickinson, Le Pont-De-Claix, France) working with an argon laser (emission wavelength at 488 nm). For each analysis, at least 10000 events were counted.

4.8. Results and Discussion

4.8.1 Doxorubicin loaded polymersomes (PolyDOX)

Doxorubicin HCl (DOX), (Figure 4.1), an anthracycline antibiotic with antineoplastic activity was used as model drug to investigate potentiality of novel $PBLG_{23}$-*b*-HYA_{10} polymersomes for therapeutical applications.

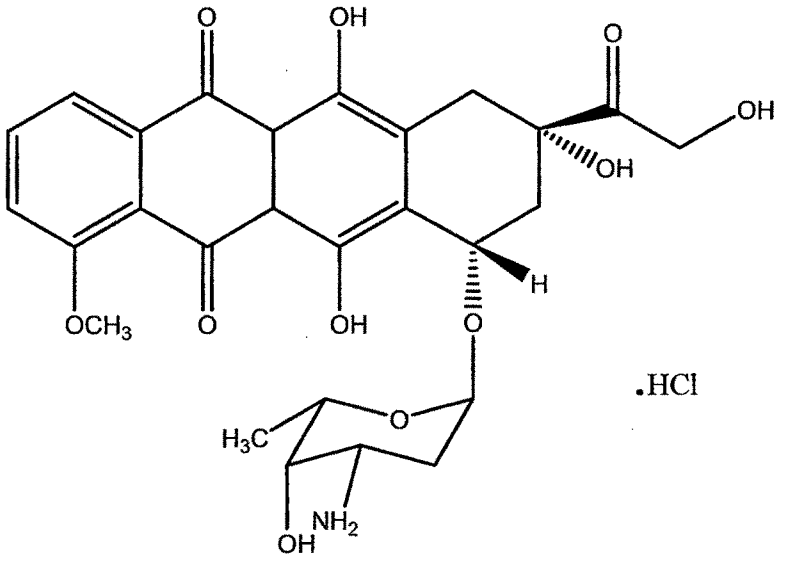

Figure 4.1 Doxorubicin HCl (Mw = 580 g/mol).

DOX salt is freely soluble in water and DMSO. Therefore DOX calibration curves have been plotted in tris buffer (10 mM, 154mM ionic strength with pH=7.4), in acetate buffer (pH = 5.5) (Figure 4.2A) and also in DMSO: Tris buffer (80:20) (Figure 4.2B) for further use in DOX estimation at λ_{max} = 485nm.

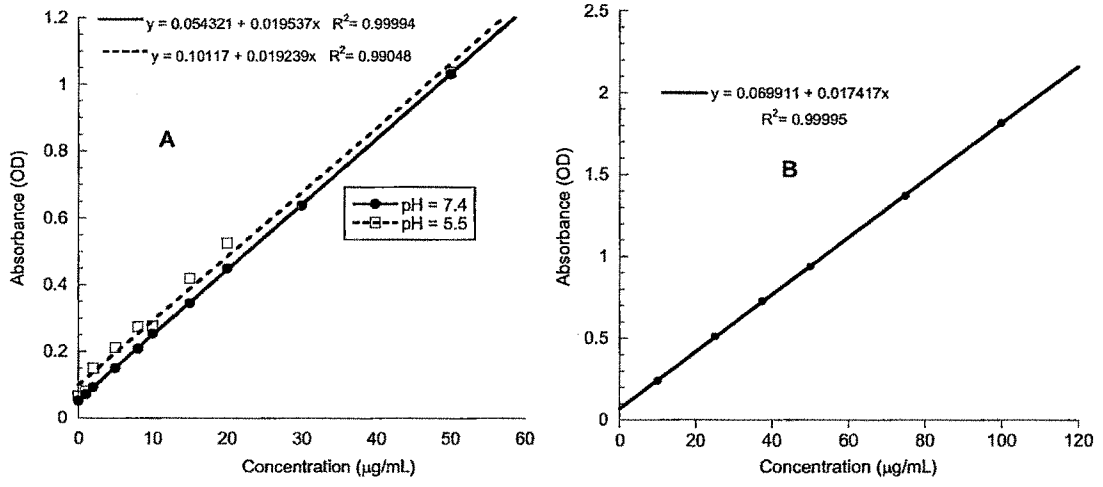

Figure 4. 2 (A) Calibration curve of DOX in tris buffer (pH = 7.4) and in acetate buffer (pH = 5.5), (B) Calibration curve of DOX in DMSO: Tris buffer (80:20).

However, DOX exhibits a pH dependent stability. DOX is not stable in aqueous solutions at physiological pH but is rather stable at low pH (3-4) and in non-aqueous

solution (European Patent EP0372888; European Patent EP0299528). Figure 4.3 represents the time dependent stability of DOX at pH 7.4 in tris buffer.

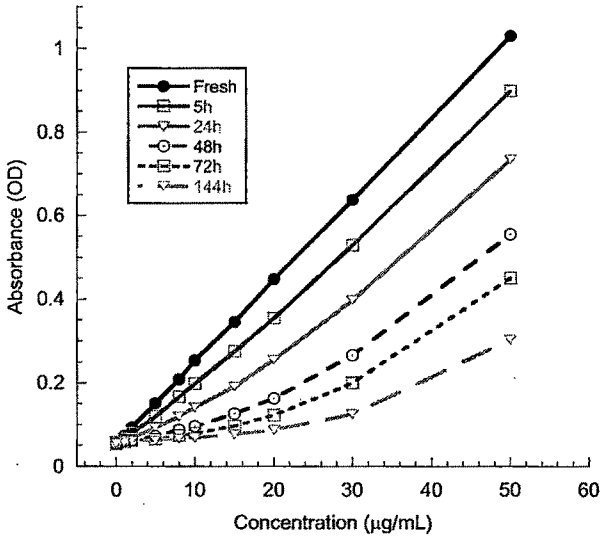

Figure 4.3 Time dependent stability of DOX in tris buffer (10 mM, 154mM ionic strength with pH = 7.4). (Absorbance at λ_{max} =485nm)

DOX loading was performed at different feed weight ratios (drug/copolymer) by a so called nanoprecipitation method. Table 4.1 represents the loading content at different feed weight ratios. The drug in excess was removed by dialysis against Tris buffer (10 mM, 154mM ionic strength with pH = 7.4). The drug loading content and drug loading efficiency were determined by spectrophotometry. The maximum DOX loading in polymersomes that has been achieved was 12±1 wt% (i.e. 120µg of drug/mg of vesicles) with encapsulation efficiency of about 40% at weight ratio 0.3/1.0 (drug/copolymer).

Table 4.1 Loading content of PolyDOX at different feed weight ratios of DOX/block copolymer*

DOX/PBLG-*b*-HYA (weight ratio)	Drug loading Content (%)	Drug loading Efficiency (%)	radius (nm)
0.1:1	4.9 ± 0.5	50 ± 5	222
0.2:1	9.7 ± 0.9	49 ± 5	212
0.3:1	12 ± 1	40 ± 4	217

* Each value is the mean (±S.D.) of three experiments (n=3).

Dynamic light scattering experiments was performed at different angles (Figure 4.4A). A hydrodynamic radius R_H of 220nm was measured with one main narrow relaxation time distribution and a low polydispersity from cumulant analysis (Table 4.1 and Figure 4.4A). In addition, the linear fitting of Γ, the relaxation frequency, versus q^2, the squared scattering vector, passing through the origin is the hallmark of a translational diffusive process, confirming the presence of spherical objects (Figure 4.4B). The hydrodynamic radius did not vary in a large extent between different batches which demonstrated the reproducibility of the preparation method. In addition, UV-vis spectra of free DOX, polymersomes and PolyDOX were recorded. UV-vis spectrum of DOX presented a maxima (Figure 4.5) at λ= 485nm. Uv-vis spectrum of polymersomes shows a sharp decrease from 200 nm to 800 nm. It is clear from different batches of PolyDOX with an increasing feed weight ratio of DOX/copolymer that the observed increase in absorbance at 485 nm is related to a higher amount of DOX loaded.

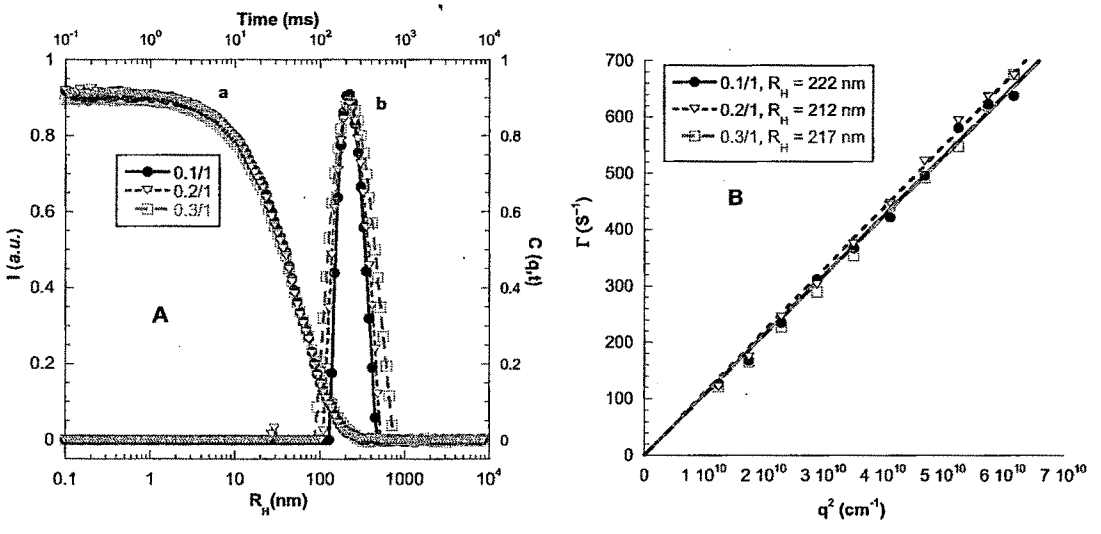

Figure 4.4 DLS of PolyDOX at different feed weight ratios of DOX/copolymer. (A) DLS autocorrelation function of PolyDOX (a) and (b) their time relaxation distribution at 90° scattering angle. (B) Decay rate (Γ) dependency to the squared scattering vector q^2.

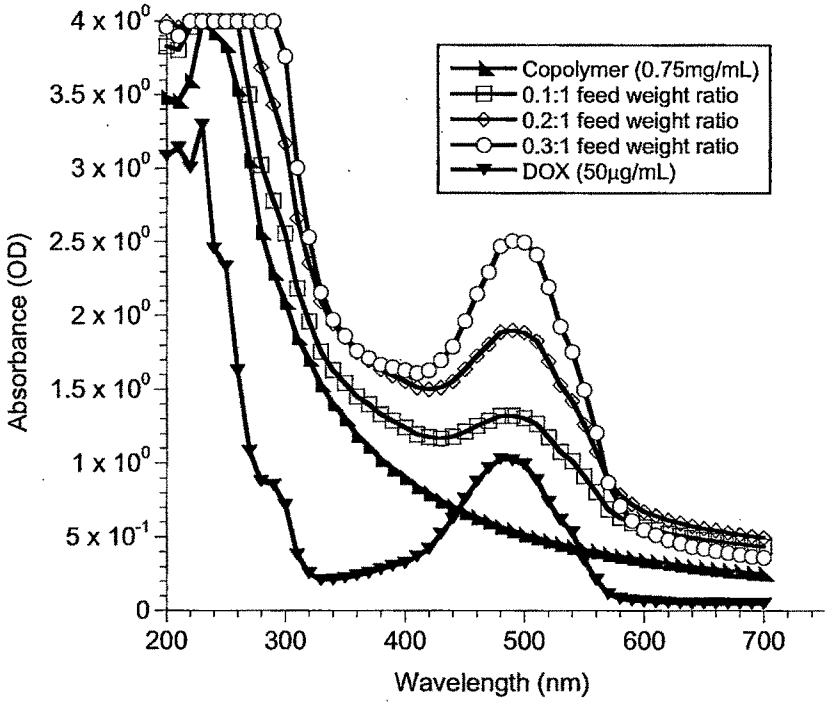

Figure 4.5 UV-vis spectra of free DOX, polymersomes before and after loading of DOX at different feed weight ratios of DOX/copolymer.

Morphology and characteristic sizes of polymersomes remained unaffected after loading. It is worthwhile to note that the morphology and the size of the vesicles remained constant after loading as illustrated in TEM, FF-TEM (Figure 4.6 A and B) and AFM analysis (Figure 4.7 and 4.8). The AFM image (Figure 4.7) is particularly interesting, compared to the one before loading (Chapter III), as it shows a dense core, due to the presence of DOX into the vesicle reservoir. Figure 4.8 represents the AFM cross-section analysis of selected vesicles.

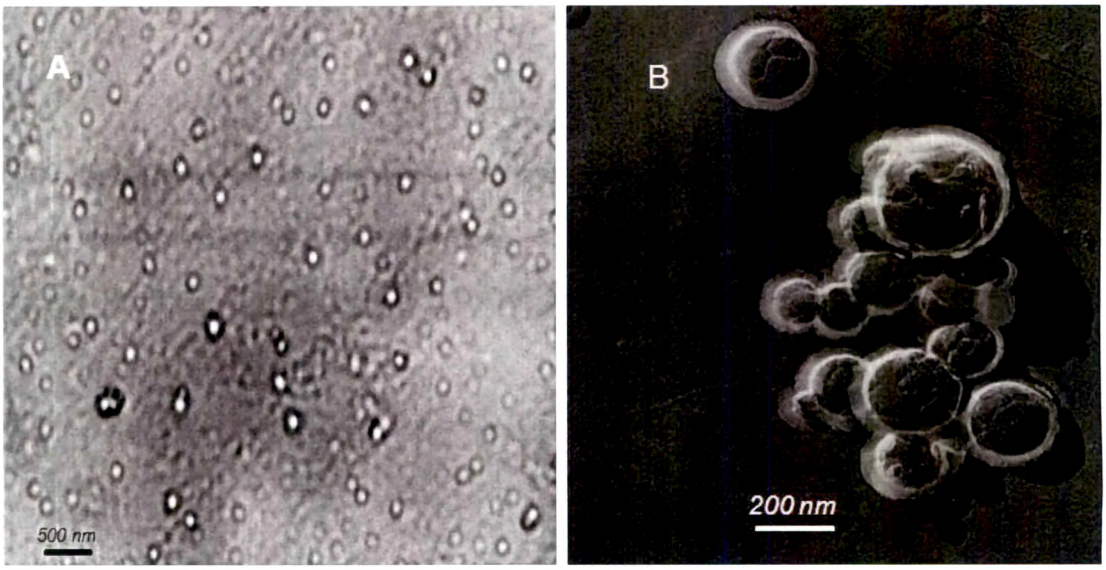

Figure 4.6 Electron microscopy of PolyDOX. (A) TEM and (B) FF-TEM.

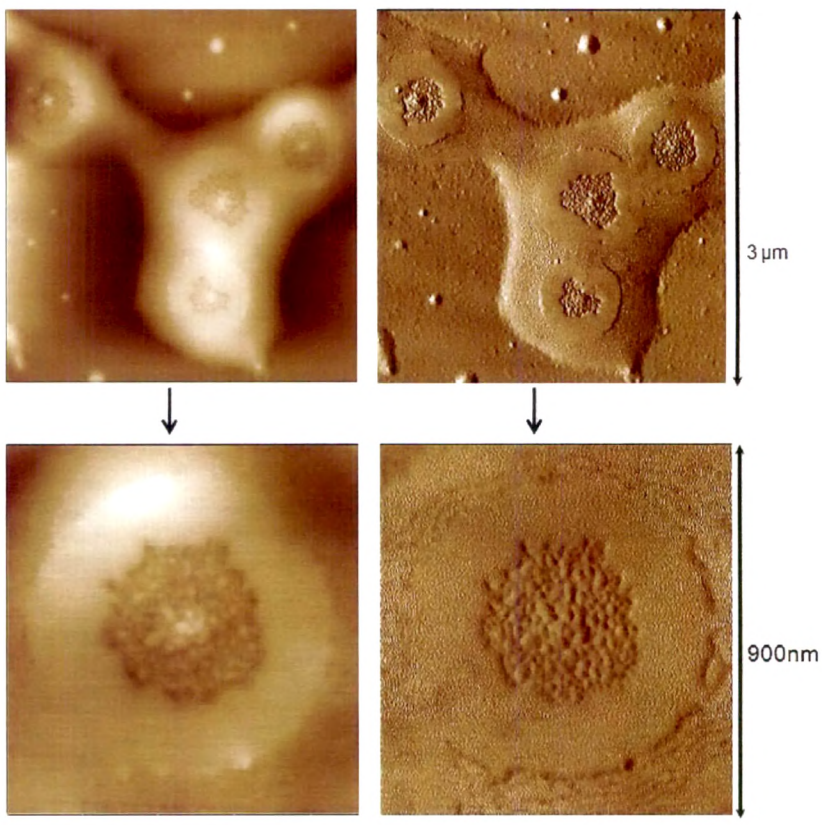

Figure 4.7 AFM analysis of PolyDOX.

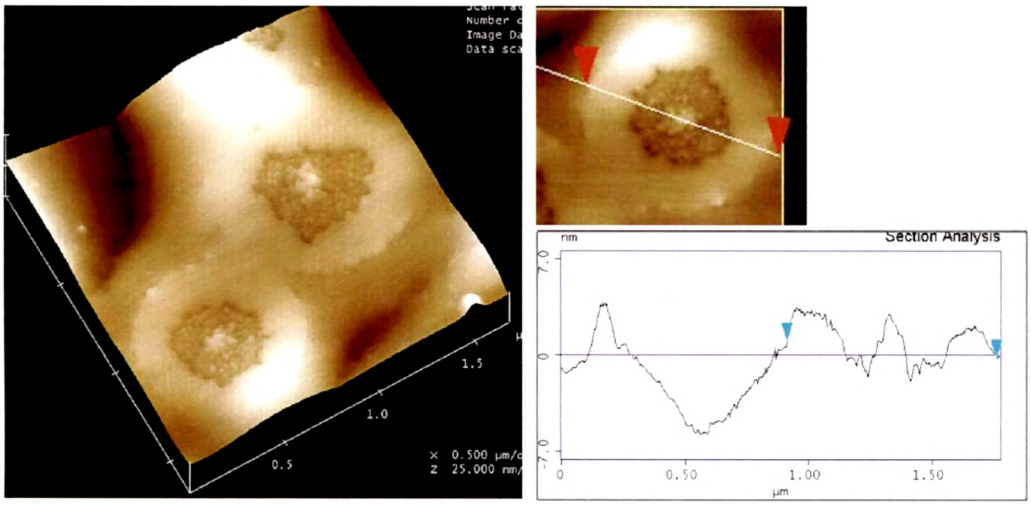

Figure 4.8 Section analysis in AFM image of selected PolyDOX.

Furthermore, PolyDOX stability was examined at different pHs for their particle size and zeta potential (Figure 4.9). DOX encapsulation in polymersomes did not affect their colloidal stability since the hydrodynamic radius of polymersomes is the same with and without DOX whatever the pH. The protonation of acid functions at low pHs, below the pKa, decreases the surface charge density as stated by the increase in zeta potential. As a consequence, polymersomes are less stable and start to aggregate (see the increase in size below pH 3).

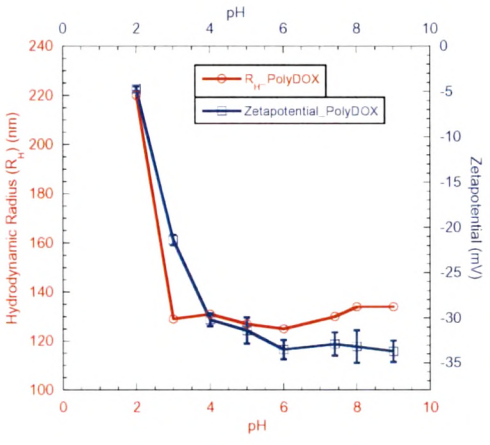

Figure 4.9 Effect of pH on the zeta potential and hydrodynamic radius of PolyDOX after sonication.

One of the known properties of polymersomes is their capacity to encapsulate hydrophilic molecules within their lumen and also integrate hydrophobic molecules within the membrane. Due to the solubility of DOX in both water and DMSO, DOX can be incorporated in the vesicle membrane as well as in lumen. Free DOX was completely released in 8h at pH 7.4 whereas $PBLG_{23}$-*b*-HYA_{10} based polymersomes modify the *in vitro* release pattern of DOX after encapsulation at pH 5.5 or 7.4 (Figure 4.10A).

Figure 4.10 illustrate DOX release profile in the acetate buffer pH 5.5 and tris buffer pH 7.4 medium, which indicates a biphasic release pattern, similar for both pH conditions. Time for 50% DOX release was around 24h at both pH, and remaining DOX released up to 10 days. *In vitro* sustained release behavior of DOX has been reported from hyaluronic acid coated DOX nanocarriers (HCDCs) and it release 80% DOX in 14days (Hyung et al., 2008). It could be the advantageous feature of this polymersomes where initial high drug release provides an initial dose followed by a controlled release in therapy. The release of the DOX from the polymersomes could be mostly driven by diffusion through the bilayer membrane. Fitting of the experimental data was assessed using well known release kinetics models (Tiwari et al., 2009) such as zero order ($M_t = M_\infty kt$), first order ($M_t = M_\infty e^{kt}$), Higuchi model ($M_t = M_\infty kt^{1/2}$) and Korsmeyer-peppas ($M_t = M_\infty kt^n$), where M_t and M_∞ represent mass release at time (t) and at infinite time (∞) respectively, k is a diffusion coefficient constant and t is time for study period. None of these models was giving a good fitting over the all release profile. We have plotted the data using the Higuchi representation (Figure 4.11), that showed two linear domains in the release curve. This representation confirmed a two step release profile with two kinetic constants.

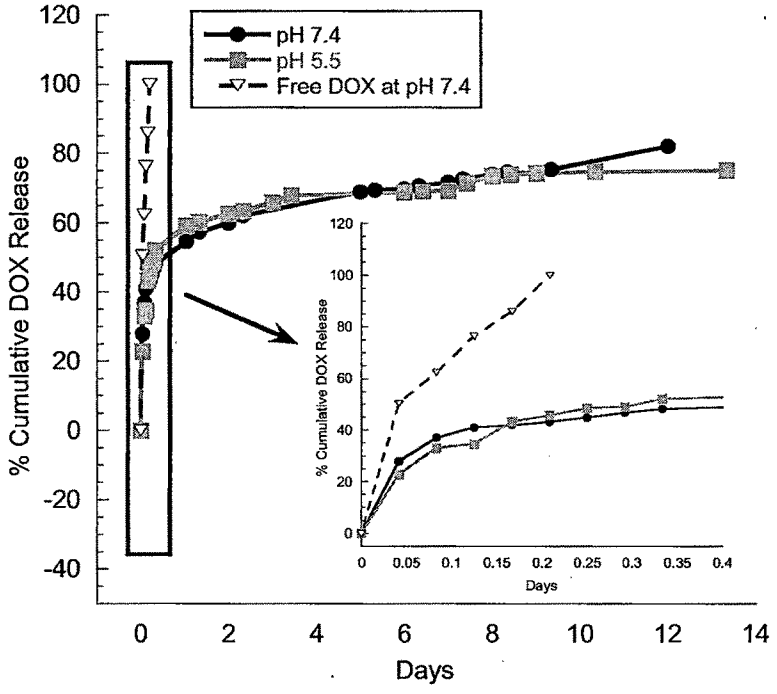

Figure 4.10 *In vitro* release patterns of free DOX and loaded DOX at pH 5.5 and 7.4.

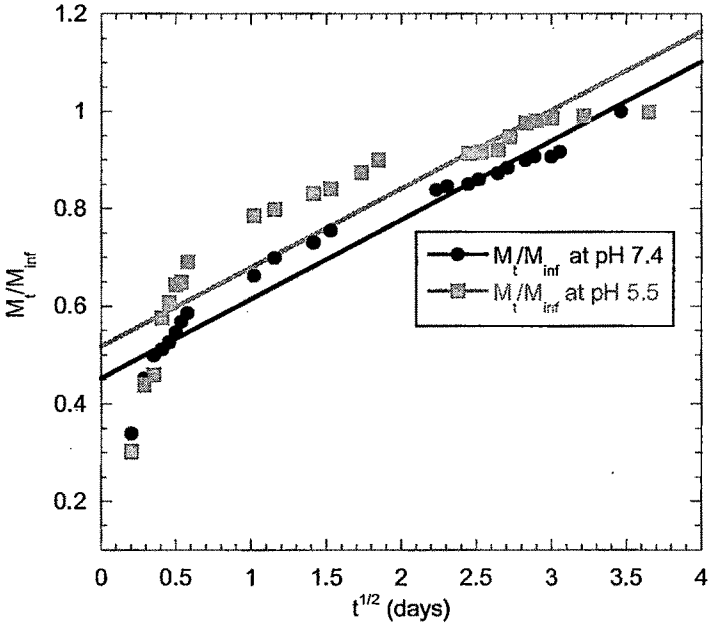

Figure 4.11 Higuchi representations of *in vitro* release profiles of PolyDOX at pH 5.5 and 7.4.

Stability of PolyDOX formulations was investigated at both RT and at 4^0C to determine the effect of storage conditions on the loading content and hydrodynamic radius (R_H) (Table 4.2). The hydrodynamic radius (R_H) was not affected by the storage for 120 days, excepted that loose aggregates are formed at 4^0C but they disappear after one minute of vortexing. However, a significant difference in loading content was observed at storage conditions RT and 4^0C. Above than 90% DOX was recovered from each PolyDOX formulation after being storage at 40^0C for 120 days whereas less than 90% DOX was obtained in each PolyDOX formulation in 15 day's storage at RT in open area (Table 4.2). The stability of PolyDOX formulations was enhanced by lyophilization process. As we have already discussed in chapter III, the presence of 40% wt of hyaluronan in polymersomes act as cryoprotectant in lyophilization process and protect the vesicular morphology after reconstitution in aqueous solutions. There was no significant difference in loading content before and after lyophilization storage at 4^0C for six months but a slight increase in size was observed as for blank polymersomes (chapter III) (Figure 4.12). Full redispersion of lyophilized vesicles was achieved in tris buffer by vortexing for 10min. We also used a very low power sonication bath for 30 seconds in order to accelerate the dispersion time and eventually eliminate the few aggregates still present in solution.

Table 4.2 Stability study of PolyDOX at RT and 4^0C

PolyDOX Formulations at different %wt ratios of DOX/copolymer	Particle size (nm)			Loading content (%)		
	0 day	After 120 days		0 day	After 120 days	After 15 days
	RT*	4±1^{0}C	RT		4±1^{0}C	RT
0.1/1	222	230	221	4.9±0.5	4.7±0.3	4.3±0.5
0.2/1	212	227	220	9.7±0.9	9.4±1.2	8.2±0.8
0.3/1	217	210	215	12±1.0	11.6±0.9	9.7±0.9

*RT = Room temperature (25 ± 2^{0}C)

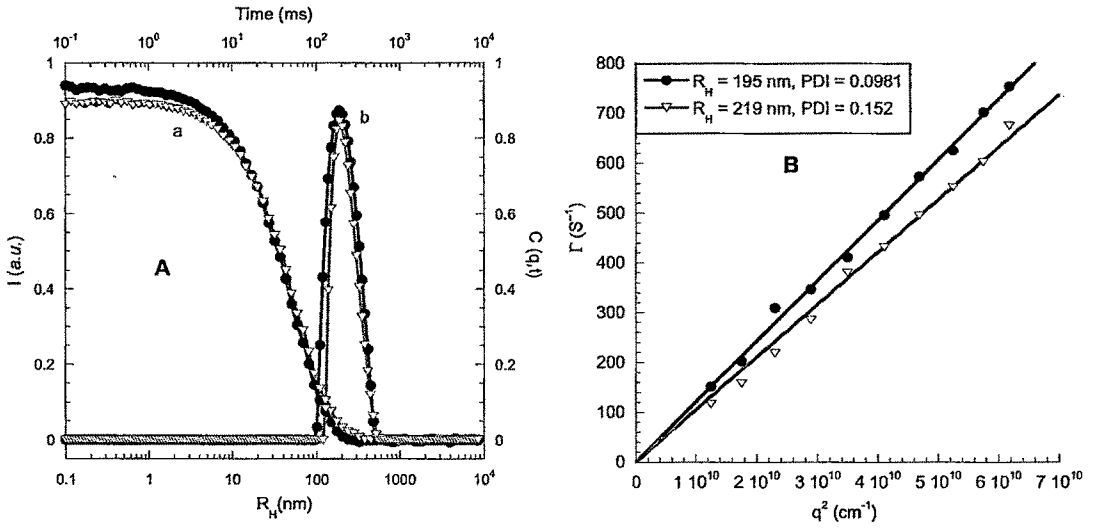

Figure 4.12 (A) DLS autocorrelation function (a) of the PolyDOX before (black line) and after reconstitution of lyophilized PolyDOX (light black line) and (b) their time relaxation distribution at 90° scattering angle. (B) Decay rate Γ dependency to the square scattering vector q^2.

4.8.2 *In vitro cell line studies on C6 rat glioma cancer cell*

The first and most readily noticeable effect following exposure of cells to toxic materials is the alteration in cell shape or morphology in a monolayer culture. Microscopic observations of treated cells showed distinct morphological changes indicating unhealthy cells, whereas the control appeared normal (Figure 4.13A, D). These phase contrast images (Figure 4.13) showed clearly different interactions of C6 cells with free DOX and PolyDOX at 3 and 24h. Free DOX treated cells appeared compact with almost same morphology as control at 3h (Figure 4.13 B) because of diffusion mediated internalization in C6 cells and also it could be the lag phase for DOX killing on C6 cells whereas at 24h with DOX, round cells that could be dead cells with cluster of cells appeared (Figure 4.13C). However, PolyDOX treated cells appeared to be clustered with cellular extensions and external buds were observed as compared to control cells, it could be due to receptor mediated endocytosis uptake.

The cytotoxicity of PolyDOX was evaluated in C6 glioma tumor cell lines looking at the dehydrogenase activity with the MTT assay. In addition, C6 cells are expressing CD44 receptors at their surface (Tsatas et al., 2002) that should help the hyaluronan-based polymersomes internalization via endocytosis (Palyi-Krekk et al., 2008). Control

$PBLG_{23}$-*b*-HYA_{10} polymersomes without drug did not show a cytotoxic effect in the concentration range 0.1 – 700μg/mL. Then, the effect of DOX concentration as well as the incubation time was studied. It is worthwhile to mention that the DOX concentration in polymersomes was adjusted to the same as that of free drug. Figure 4.14 represents the time course of the fall in half maximal inhibitory concentration (IC_{50}) at 17μM equivalent to DOX concentration and it represents also the idealized curve for DOX and PolyDOX with progressive increase in cytotoxicity with time but eventually reaching a maximum effect after three cycles (Initial cytotoxicity, slope and plateau).

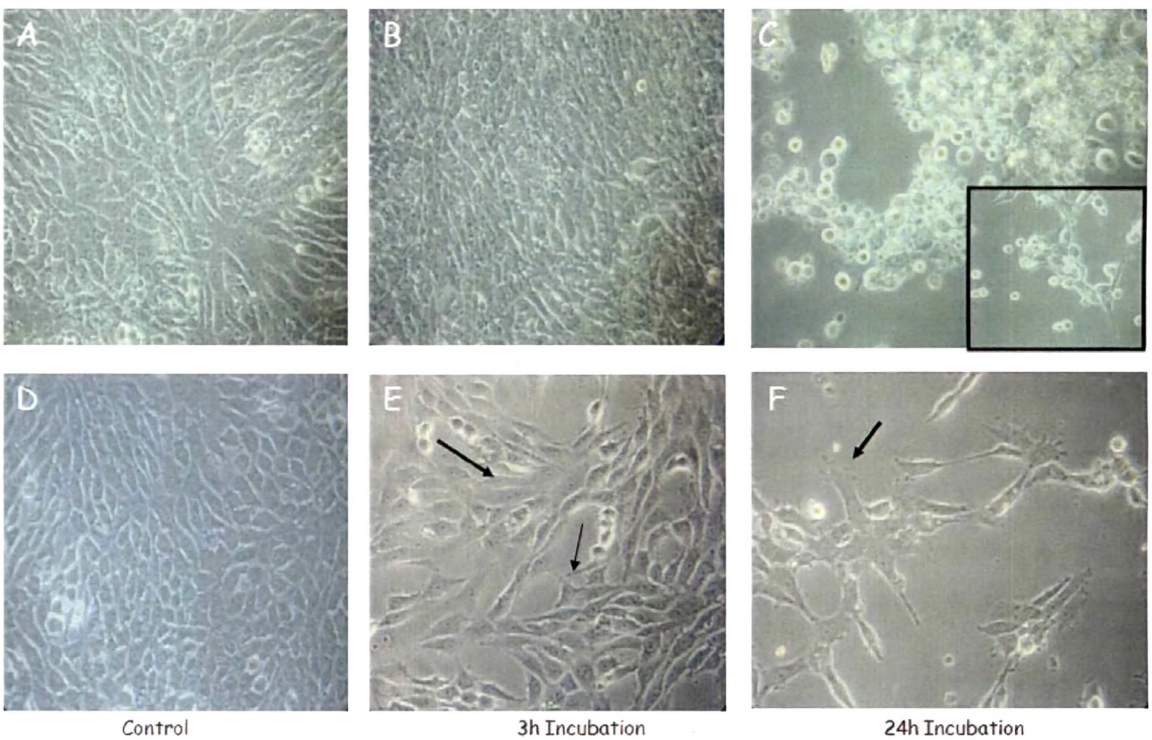

Figure 4.13 Phase contrast images of C6 cells after treatment with free DOX and PolyDOX. Fig. A, B and C are C6 glioma cells incubated with and without free DOX (5 μM) incubated at 3, and 24h. Fig. D, E and F are C6 glioma cells incubated with and without PolyDOX (5 μM DOX concentration) incubated at 3, and 24h. Inset in C is representative of aggregated and ovoid cells. On Figure E, the thin arrow represents a typical membrane bud of activated C6 cells and the bold arrow shows both elongated and ovoid morphology of C6 cells. Figure F, arrow represent buds on the activated C6 cells. Magnification 40 ×.

Table 4.3 represents IC_{50} values of free DOX and PolyDOX. It is clear that IC_{50} of free DOX and loaded DOX was time-dependent. At 48h, free DOX produces IC_{50} = 1μM whereas PolyDOX have IC_{50} = 7.63μM. This difference could be explained by different

internalization mechanism (Figure 4.13, 4.15) as it will be further explained later. Cytotoxicity measurement at 48h, performed at 5 μM concentration, showed that cells incubated with free DOX are strongly affected (80% death), while cells incubated with PolyDOX are unaffected.

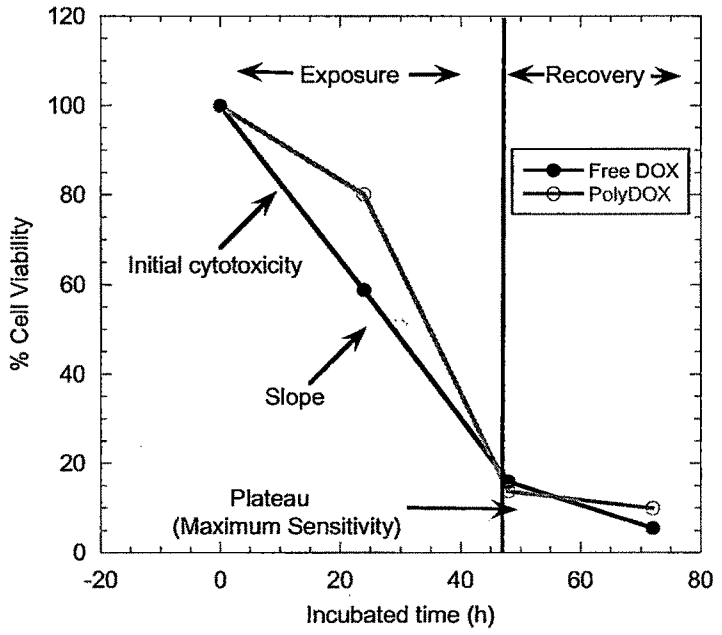

Figure 4.14 Cell viability (%) at different incubation time with free DOX (17μM) and PolyDOX (17μM).

Table 4.3 *In Vitro* half maximal inhibitory concentration (IC_{50}) values measured for free DOX and PolyDOX on C6 cells at different incubation time

Incubation Time (h)	IC_{50} (μM)	
	Free DOX	PolyDOX
24h	20.91	-*
48h	1.0	7.53
72h	0.16	2.76

** Value not measurable*

To get more insight, cytotoxic cell uptake studies were performed with free and DOX-loaded vesicles (Figure 4.15). Indeed after 24h incubation with free DOX (5μM), cells changed their morphology, being retracted and ovoids, and losing their adhesion properties (Figure 4.15a, c). These observations are typical for cells engaged in death

processes, probably by apoptosis, as known with DOX. However, for similar incubation conditions with PolyDOX, most of the cells still spread and stick on the culture support (Figure 4.15b, d). Furthermore, DOX fluorescence allows for visualisation of the drug distribution in the still living cells, either by microscopy or cytometry. After 24h incubation, fluorescence was observed for free DOX, in the cytoplasm and mostly in the nucleus of the round cells (Figure 4.15c). Under the same conditions, the PolyDOX fluorescence appeared more diffuse in the cytoplasm and particularly concentrated as dots in endosomal like vesicles (Figure 4.15d inset). These images not only show that PolyDOX are an efficient carrier to bring DOX into the cytoplasm, but also propose that the internalization mechanism of polymersomes is different from that of free DOX which is accumulated by the cells following unspecific diffusion process. Similar results were reported by Gao and coworkers in MCF-7 cell lines with poly(ethylene oxide)-*b*-poly(ε-caprolactone) micelles (Shuai et al., 2004). This noticeable difference at intracellular level or in sub-cellular distribution of DOX suggests that PolyDOX were taken up by cells mainly via an endocytic pathway.

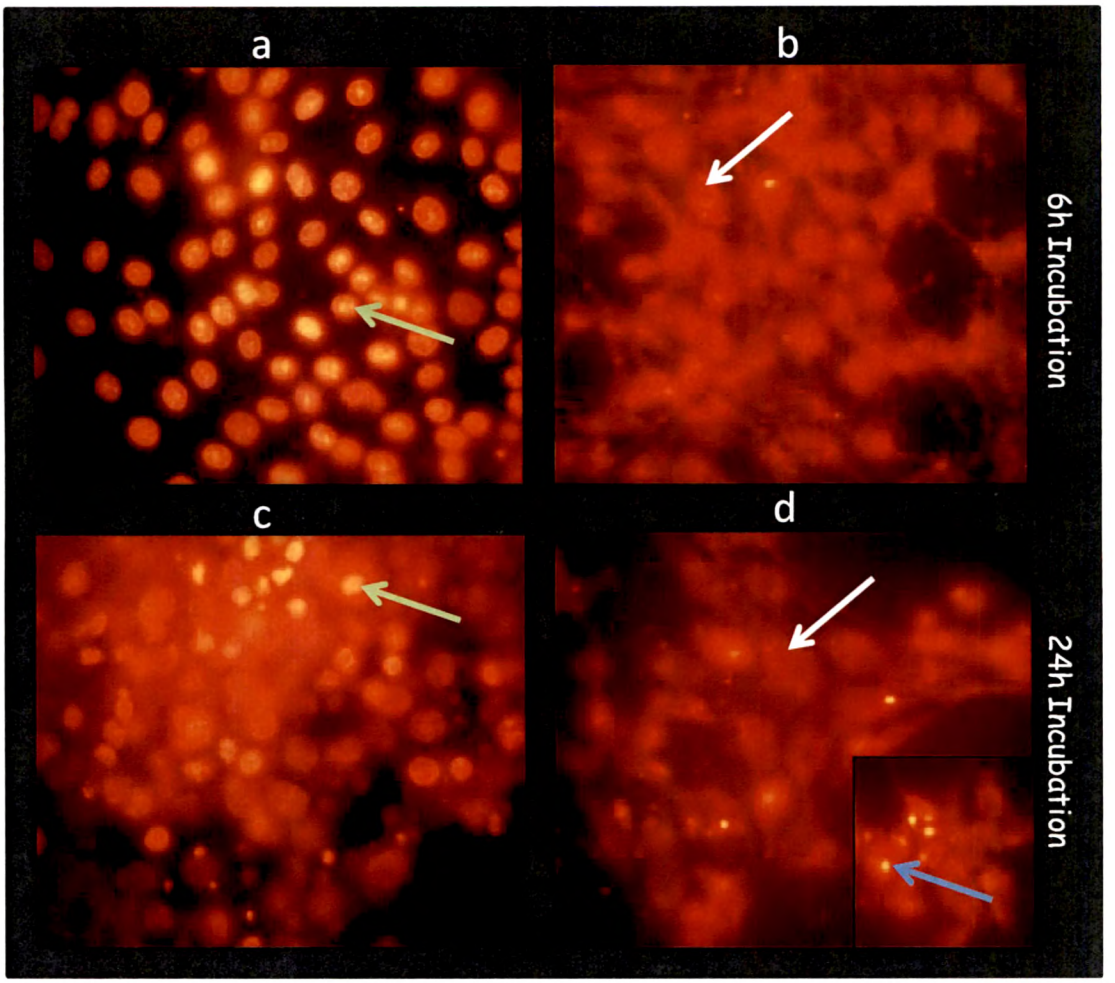

Figure 4.15 Fluorescence images of C6 glioma tumor cells incubated with free DOX (a and c) and PolyDOX (b and d) incubated for 6h and 24h. Green arrows are showing accumulation of DOX in the nucleus and DNA fragmentation. White arrows are demonstrating nucleus with no or low amount of DOX when incubated with PolyDOX. Blue arrow is revealing accumulation of PolyDOX in endosomal like cellular vesicles.

The cytometry analysis, performed only on living cells, showed a similar level of the cell fluorescence, independently of its intracellular location as seen by microscopy (Figure 4.16a). However, the large profile of fluorescence after 6h incubation of free DOX is in contrast with the thinner and higher level of fluorescence measured for PolyDOX. This difference could be relevant of a diffuse intracellular repartition of DOX, being both located in the cytoplasm and the nucleus for free DOX incubation (as observed by microscopy), opposed to a more localized concentration of PolyDOX in the cellular vesicle compartments. For 24h time point, the cytometry profile of free DOX

incubated cells is in agreement with a nuclear accumulation. Moreover, the concerned cell number decreased faster for cells in the free DOX conditions, than for ones incubated with PolyDOX (Figure 4.16b).

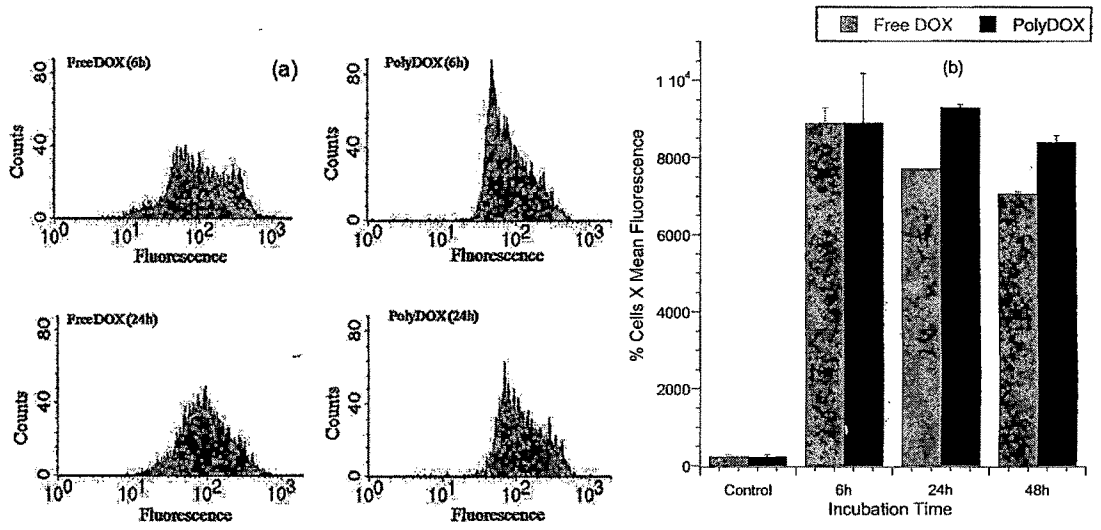

Figure 4.16 (a) Cytometry analysis of C6 glioma tumor cells incubated with free DOX and PolyDOX for 6h and 24h. (b) Evolution of the global fluorescence with incubation time for free DOX and PolyDOX. This parameter is representative of the level of the fluorescent still living C6 population.

As a result, the time evolution of the global fluorescence per condition (Figure 4.16b) showed a lag of 24h in its decrease, being the consequence of the PolyDOX compartmentalization. Indeed, this delay is representative of time involved for the shift of the DOX from the PolyDOX, and then from endosomal like vesicles to the cytoplasm, before its accumulation inside the nucleus when interacting with the DNA. Then, the viability decreased in both conditions with a similar evolution. In conclusion, the internalization of the DOX inside targeting polymersomes delayed the apoptosis action of the drug without affecting its efficiency due to the polymersomes endosomal internalization. Finally, the cellular vesicle accumulation of PolyDOX strongly suggests an endocytosis pathway, probably receptor mediated.

4.9. Conclusion

We found that block copolymers composed of a polypeptide segment and a polysaccharide moiety provide significant advantages in controlling both the vesicular

structure and the biofunctionality. Such biomimetic self-assemblies combine high colloidal stability, biocompatibility and degradability, together with controlled release properties of drugs. The use of hyaluronan as the hydrophilic stabilizing block, combined to its specific ligand properties to CD44 glycoprotein receptors that are over-expressed in many cancers, provides a means to obtain synergy between structure and biofunctionality within a single material. Such an original approach opens new avenues in the preparation of multifunctional nanodevices.

References

- Adams DJ, Adams S, Atkins D, Butler MF, Furzeland S. Impact of Mechanism of Formation on Encapsulation in Block Copolymer Vesicles. J Control Release 2008;128(2):165-70.
- Ahmed F, Pakunlu RI, Brannan A, Bates F, Minko T, Discher DE. Biodegradable polymersomes loaded with both paclitaxel and doxorubicin permeate and shrink tumors, inducing apoptosis in proportion to accumulated drug. J Control Release 2006;116(2):150-8.
- Ahmed F, Pakunlu RI, Srinivas G, Brannan A, Bates F, Klein ML, Minko T, Discher DE. Shrinkage of a Rapidly Growing Tumor by Drug-loaded Polymersomes: pH-triggered release through copolymer degradation. Mol Pharma 2006;3(3):340–50.
- Bellomo EG, Wyrsta MD, Pakstis L, Pochan DJ, Deming TJ. Stimuli-responsive polypeptide vesicles by conformation-specific assembly. Nat Mater 2004;3(4):244-8.
- Bermudez H, Brannan AK, Hammer DA, Bates FS, Discher DE. Molecular weight dependence of polymersome membrane structure, elasticity, and stability. Macromolecules 2002;35,8203-08.
- Calnan BJ, Tidor B, Biancalana S, Hudson D, Frankel AD. Arginine-mediated RNA recognition: the arginine fork. Science 1991;252(5010):1167-71 .

- Discher BM, Won Y-Y, Ege DS, Lee JC-M, Bates FS, Discher DE, Hammer DA. Polymersomes: Tough vesicles made from diblock copolymers. Science 1999;284(5417),1143-46.
- Discher DE, Eisenberg A. Polymer vesicles. Science 2002;297(5583),967-73.
- Discher DE, Ortiz V, Srinivas G, Klein ML, Kim Y, Christian D, Cai S, Photos P, Ahmed F. Emerging Applications of Polymersomes in Delivery: From Molecular Dynamics to Shrinkage of Tumors. Prog Polym Sci 2007;32,838–57.
- Eliaz RE, Szoka FC Jr. Liposome-encapsulated doxorubicin targeted to CD44: A strategy to kill CD44-overexpressing tumor cells. Cancer Res 2001;61(6):2592-601.
- European Patent EP0299528. Doxorubicin hydrochloride nonaqueous solution. Bristol-Myers Squibb Company. 345 Park Avenue, New York, N.Y., 10154, US.
- European Patent EP0372888. Doxorubicin aqueous solutions. Bristol-Myers Squibb Company. 345 Park Avenue, New York, N.Y., 10154, US.
- Farokhzad OC, Langer R. Impact of nanotechnology on drug delivery. ACS Nano 2009;3,16-20.
- Ghoroghchian PP, Frail PR, Susumu K, Blessington D, Brannan AK, Bates FS, Chance B, Hammer DA, Therien MJ. Near-Infrared-Emissive Polymersomes: Self-Assembled Soft Matter for In Vivo Optical Imaging. Proc Natl Acad Sci 2005;102(8):2922-7.
- Girish KS, Kemparaju K. The magic glue hyaluronan and its eraser hyaluronidase: A biological overview. Life Sci 2007;80(21):1921-43.
- Hammer DA, Robbins GP, Haun JB, Lin JJ, Qi W, Smith LA, Ghoroghchian PP, Therien MJ, Bates FS. Leuko-polymersomes. Faraday Discuss 2008;139,129–41.
- Holowka EP, Sun VZ, Kamei DT, Deming TJ. Polyarginine segments in block copolypeptides drive both vesicular assembly and intracellular delivery. Nat Mater 2007;6(1):52-7.

- Hu Z, Sun Y, Garen A. Targeting tumor vasculature endothelial cells and tumor cells for immunotherapy of human melanoma in a mouse xenograft model. Proc Natl Acad Sci 1999;96(14):8161-6.
- Hyung W, Ko H, Park J, Lim E, Park SB, Park YJ, Yoon HG, Suh JS, Haam S, Huh YM. Novel hyaluronic acid (HA) coated drug carriers (HCDCs) for human breast cancer treatment. Biotechnol Bioeng 2008;99(2):442-54.
- Immordino ML, Dosio F, Cattel L. Stealth liposomes: review of the basic science, rationale, and clinical applications, existing and potential. Int J Nanomedicine 2006;1(3):297-315.
- Langer R. Drug delivery and targeting. Nature 1998;392,5-10.
- Lewanski CR, Stewart S. Pegylated liposomal adriamycin: A review of current and future applications. Pharm Sci Technolo Today 1999;2(12):473-477.
- Nasongkla N, Bey E, Ren J, Ai H, Khemtong C, Guthi JS, Chin SF, Sherry AD, Boothman DA, Gao J. Multifunctional polymeric micelles as cancer-targeted, MRI-ultrasensitive drug delivery systems. Nano Lett 2006;6(11):2427-30.
- Opsteen JA, Brinkhuis RP, Teeuwen RLM, Loewik DWPM, van Hest JCM. "Clickable" Polymersomes. Chem Commun 2007; 3136–38.
- Pályi-Krekk Z, Barok M, Kovács T, Saya H, Nagano O, Szöllosi J, Nagy P. EGFR and ErbB2 are functionally coupled to CD44 and regulate shedding, internalization and motogenic effect of CD44. Cancer Lett 2008;263(2):231-42.
- Peer D, Karp JM, Hong S, Farokhzad OC, Margalit R, Langer R. Nanocarriers as an emerging platform for cancer therapy. Nat Nanotechnol 2007;2(12):751-60.
- Peer D, Margalit R. Loading mitomycin C inside long circulating hyaluronan targeted nano-liposomes increases its antitumor activity in three mice tumor models. Int J Cancer 2004;108(5):780-9.
- Peer D, Margalit R. Tumor-targeted hyaluronan nanoliposomes increase the antitumor activity of liposomal doxorubicin in syngeneic and human xenograft mouse tumor models. Neoplasia 2004;6(4):343-53.

- Rodríguez-Hernández J, Lecommandoux S. Reversible inside-out micellization of pH-responsive and water-soluble vesicles based on polypeptide diblock copolymers. J Am Chem Soc 2005;127(7):2026-7.
- Shuai X, Ai H, Nasongkla N, Kim S, Gao J. Micellar carriers based on block copolymers of poly(epsilon-caprolactone) and poly(ethylene glycol) for doxorubicin delivery. J Control Release 2004;98(3):415-26.
- Sun G, Fang H, Cheng C, Lu P, Zhang K, Walker AV, Taylor JS, Wooley KL. Benzaldehyde-functionalized polymer vesicles. ACS Nano 2009;3(3):673-81.
- Tiwari A, Bindal S, Bohidar HB. Kinetics of protein-protein complex coacervation and biphasic release of salbutamol sulfate from coacervate matrix. Biomacromolecules 2009;10(1):184-9.
- Tsatas D, Kanagasundaram V, Kaye A, Novak U. EGF receptor modifies cellular responses to hyaluronan in glioblastoma cell lines. J Clin Neurosci 2002;9(3):282-8.
- Whitesides GM. the "Right" Size in Nanobiotechnology. Nat Biotechnol 2003;21,1161-65.
- You L, Schlaad H. An Easy Way to Sugar-Containing Polymer Vesicles or Glycosomes. J Am Chem Soc 2006;128(41):13336-7.